Comparison of three seemingly similar lytic polysaccharide monooxygenases from *Neurospora crassa* suggests different roles in plant biomass degradation

Received for publication, February 27, 2019, and in revised form, August 2, 2019 Published, Papers in Press, August 20, 2019, DOI 10.1074/jbc.RA119.008196

Dejan M. Petrović[‡], Anikó Várnai[‡1], Maria Dimarogona[§¶], Geir Mathiesen[‡], Mats Sandgren[§], Bjørge Westereng[‡], and Vincent G. H. Eijsink[‡]

From the [‡]Faculty of Chemistry, Biotechnology and Food Science, Norwegian University of Life Sciences (NMBU), 1432 Ås, Norway, [§]Department of Molecular Sciences, Swedish University of Agricultural Sciences, 75007 Uppsala, Sweden, and [¶]Laboratory of Biotechnology and Structural Biology, Department of Chemical Engineering, University of Patras, 26504 Patras, Greece

Edited by Gerald W. Hart

Many fungi produce multiple lytic polysaccharide monooxygenases (LPMOs) with seemingly similar functions, but the biological reason for this multiplicity remains unknown. To address this question, here we carried out comparative structural and functional characterizations of three cellulose-active C4-oxidizing family AA9 LPMOs from the fungus *Neurospora crassa*, *Nc*LPMO9A (NCU02240), *Nc*LPMO9C (NCU02916), and *Nc*LPMO9D (NCU01050). We solved the three-dimensional structure of copper-bound *Nc*LPMO9A at 1.6-Å resolution and found that *Nc*LPMO9A and *Nc*LPMO9C, containing a CBM1 carbohydrate-binding module, bind cellulose more strongly and were less susceptible to inactivation than *Nc*LPMO9D, which lacks a CBM. All three LPMOs were active on tamarind xyloglucan and konjac glucomannan, generating similar products but clearly differing in activity levels. Importantly, in some cases, the addition of phosphoric acid–swollen cellulose (PASC) had a major effect on activity: *Nc*LPMO9A was active on xyloglucan only in the presence of PASC, and PASC enhanced *Nc*LPMO9D activity on glucomannan. Interestingly, the three enzymes also exhibited large differences in their interactions with enzymatic electron donors, which could reflect that they are optimized to act with different reducing partners. All three enzymes efficiently used H_2O_2 as a cosubstrate, yielding product profiles identical to those obtained in O_2-driven reactions with PASC, xyloglucan, or glucomannan. Our results indicate that seemingly similar LPMOs act preferentially on different types of copolymeric substructures in the plant cell wall, possibly because these LPMOs are functionally adapted to distinct niches differing in the types of available reductants.

The filamentous fungus *Neurospora crassa* is commonly found in nature where it grows on dead plant material, particularly grasses. Its cellulolytic potential has been known for decades (1–3). The *N. crassa* genome encodes a similar number of glycoside hydrolase (GH)[2] enzymes as *Hypocrea jecorina*, the main industrial source of enzymes for biomass depolymerization (4). The *N. crassa* genome also encodes 14 genes encoding lytic polysaccharide monooxygenases (LPMOs) belonging to CAZy family AA9 (5). Transcriptome studies done at a time when these LPMOs were erroneously thought to be glycoside hydrolases belonging to CAZy family GH61 showed transcripts for 13 of the AA9-encoding genes (6). LPMO-encoding genes tend to be abundant in the genomes of biomass-degrading fungi, indicating an important role in biomass degradation and raising questions as to the evolutionary drivers of this high multiplicity (7–11).

LPMOs are monocopper enzymes (12, 13) that were identified in 2010 (14) and that oxidatively cleave glycosidic bonds in polysaccharides. The discovery of LPMOs has been followed by extensive research related to their structure, function, mechanism, diversity, and industrial application (11, 15–20). LPMOs have become an important ingredient of commercial enzyme mixtures for industrial biomass conversion (21–24). Although LPMO action usually is considered in light of the enzymatic deconstruction of cellulose and chitin, some LPMOs act on other substrates, including xyloglucan and other (1,4)-linked β-glucans (25, 26), starch (27, 28), and xylan (29, 30). LPMO action requires reduction of the copper by an enzymatic or nonenzymatic electron donor (9, 31, 32). Subsequently, the enzymes use either molecular oxygen (14, 33) or hydrogen peroxide (34, 35) to generate an oxygen species at the copper site

This work was supported by Norwegian Research Council Grants 214613, 244259, and 243663 (to D. M. P., A. V., B. W., V. G. H. E.) and Swedish Energy Agency Project 40144-1 (to M. S.). This work was also supported by VINNOVA (Swedish Governmental Agency for Innovation Systems Grant 2014-01453 (to M. D.). The authors declare that they have no conflicts of interest with the contents of this article.

The atomic coordinates and structure factors (code 5FOH) have been deposited in the Protein Data Bank (http://wwpdb.org/).

This article contains Table S1 and Figs. S1–S10.

[1] To whom correspondence should be addressed. Tel.: +47-6723-2569; E-mail: aniko.varnai@nmbu.no.

[2] The abbreviations used are: GH, glycoside hydrolase; AscA, ascorbic acid; CBM, carbohydrate-binding module; CDH, cellobiose dehydrogenase; HPAEC-PAD, high-performance anion-exchange chromatography with pulsed amperometric detection; KGM, konjac glucomannan; LPMO, lytic polysaccharide monooxygenase; PASC, phosphoric acid–swollen cellulose; PQQ, pyrroloquinoline quinone; PDH, pyranose dehydrogenase; TXG, tamarind xyloglucan; CAZyme, carbohydrate-active enzyme; *Nc*, *N. crassa*; *Ls*, *L. similis*; PDB, Protein Data Bank; *Mt*, *M. thermophilum*; *Cc*, *C. cinerea*; Bis-Tris, 2-[bis(2-hydroxyethyl)amino]-2-(hydroxymethyl)propane-1,3-diol; *Tr*, *Trichoderma reesei*; gem, geminal; nC, nanocoulombs; DP, degree of polymerization.

that is capable of abstracting a hydrogen atom from the C1 or the C4 of the scissile glycosidic bond.

The biological reason for the multiplicity of LPMOs remains unresolved. For example, all of the nine biochemically characterized *Nc*LPMOs (25, 36–38) are known to act on cellulose, seemingly varying only in terms of their oxidative regioselectivity: *Nc*LPMO9F (NCU03328), *Nc*LPMO9E (NCU08760), NCU02344, and *Nc*LPMO9G (NCU00836) are strictly C1-oxidizing; *Nc*LPMO9A (NCU02240), *Nc*LPMO9C (NCU02916), and *Nc*LPMO9D (NCU01050) are strictly C4-oxidizing; and *Nc*LPMO9M (NCU07898) and *Nc*LPMO9B (NCU07760) show mixed C1/C4 oxidation. For *Nc*LPMO9C, activity on other β-glucans and soluble cellodextrins has been demonstrated (25). Next to variation in oxidative regioselectivity, the LPMOs also vary in terms of the absence or presence of appended carbohydrate-binding modules (CBMs).

For more insight into potential differences between LPMOs, we have studied and compared the three strictly C4-oxidizing LPMOs of *N. crassa*, *Nc*LPMO9A (NCU02240), *Nc*LPMO9C (NCU02916) (39), and *Nc*LPMO9D (NCU01050) (37). Of these, *Nc*LPMO9A and *Nc*LPMO9C contain a family 1 carbohydrate-binding module (CBM1; known for binding both crystalline and amorphous cellulose (40, 41)). To allow structural comparisons, we solved the crystal structure of the catalytic domain of *Nc*LPMO9A. Functional analyses were inspired by the rich functional data set that was already available for *Nc*LPMO9C (25, 39, 42, 43). We have assessed properties such as substrate binding and specificity, ability to recruit electrons from enzymatic and nonenzymatic electron donors, operational stability, the ability to generate H_2O_2 in the absence of substrate (36, 42), and potential differences between O_2-driven and H_2O_2-driven catalysis.

Results

Crystal structure and initial characterization of NcLPMO9A

The three-dimensional structure of *Nc*LPMO9A with copper bound was solved to 1.6-Å resolution (Table S1) and revealed a typical LPMO structure, both with regard to the overall fold and the copper-containing active site (Fig. 1). Product analysis after incubation of *Nc*LPMO9A with phosphoric acid–swollen cellulose (PASC) using chromatographic methods (44), MS/MS analysis (42), and identification of characteristic products obtained upon reduction (33) showed that *Nc*LPMO9A exclusively oxidizes C4, confirming results of Vu *et al.* (38) (results not shown).

Overall structural comparison

Fig. 1 shows a sequence alignment and structural representations of the three C4-oxidizing LPMOs from *N. crassa*, *Nc*LPMO9A, *Nc*LPMO9C, and *Nc*LPMO9D. The pairwise sequence identities of the catalytic domains range from 50 to 60%. Regions that are believed to be involved in substrate binding in family AA9 LPMOs are known as the L2, L3, LS, and LC loops (18, 45). Apart from the L3 loop, sequence conservation in these loops is similar to sequence conservation in the rest of the protein. The L3 loop shows higher sequence variability, and both the L3 and the LC loops are somewhat shorter in *Nc*LPMO9A and *Nc*LPMO9D compared with *Nc*LPMO9C (Fig. 1*A*). Previous NMR studies on *Nc*LPMO9C have shown that His-1, Ala-80, His-83, and His-155 (Fig. 1*A*, marked with * at positions 1, 78, 81, and 153, respectively) are involved in binding of both oligocellulose and polymeric xyloglucan (46), and three of these four residues are conserved among the three *Nc*LPMOs. The residue at position 78 is predicted to take part in forming the −1 subsite (subsite prediction based on Courtade *et al.* (46) and Frandsen *et al.* (47)) varies; it is an Ala (Ala-80) in *Nc*LPMO9C and an Asp in *Nc*LPMO9A (Asp-78) and *Nc*LPMO9D (Asp-81). Superposition of the three *Nc*LPMO structures with that of an AA9 LPMO from *Lentinus similis* (*Ls*AA9A) in complex with cellohexaose (PDB code 5ACI (47)) (Fig. 2) shows that, apart from position 78, residues in subsites −1 to −3 are highly conserved among the three *N. crassa* enzymes, whereas more variation occurs in the +1 and +2 subsites as well as in the −4 subsite. These variations reside in the L2/L3 and LC regions (Fig. 1*A*) of the protein, respectively.

Courtade *et al.* (46) showed that the L3 region is involved in the interaction with xyloglucan, and both the sequence alignment and the structures (Figs. 1 and 2) show considerable variation in this region. Although Asp-76 in the L3 loop of *Nc*LPMO9C (position 74 in the alignment in Fig. 1*A*) is likely to interact with the C6-hydroxyl of the glucose unit in subsite +1, the corresponding residues in *Nc*LPMO9A (Asp-74) and *Nc*LPMO9D (Ala-77) seem not to be capable of such an interaction (Fig. 2). There is also considerable variation, *i.e.* at positions 67 and 68 in the L3 region and 25 and 26 in the L2 region. Position 68 in the L3 loop is of particular interest. The glutamate (Glu-65) in *Nc*LPMO9C is likely to contribute to substrate binding at the +2 subsite (1.9–2.2 Å from the C1- and C2-hydroxyls), similarly to Asn-67 in *Ls*AA9A (47). The side chains of the corresponding residues at this position in *Nc*LPMO9A (Thr-68) and *Nc*LPMO9D (Met-68) are less suitable to hydrogen bond with the substrate and seem to be located further away (3.7–4.4 Å) from the glucose unit in the +2 subsite. Another clear difference concerns position 25 in the L2 region where both *Nc*LPMO9A and *Nc*LPMO9D have a tyrosine, whereas *Nc*LPMO9C has an aspartate. A tyrosine could be engaged in stacking interactions with the substrate and may potentially extend the substrate-binding surface, perhaps forming a +3 subsite. The tyrosine at position 204 in the +3/+4 subsite is highly conserved in all AA9 LPMOs and well-known to be important for binding cello-oligomers (47) and xyloglucan (46). Interestingly, adjacent to this Tyr residue *Nc*LPMO9D carries a Trp (Trp-207), which could contribute to substrate binding through aromatic stacking.

Binding to PASC

Fig. 3*A* shows that in the absence of ascorbic acid (AscA) binding of all three *Nc*LPMOs reached equilibrium in 30 min after mixing with PASC. The strongest binding was observed for the two *Nc*LPMOs containing a CBM1, *Nc*LPMO9C and *Nc*LPMO9A, with ~80 and ~50% binding, respectively. Binding of *Nc*LPMO9D was much weaker, with only ~15% binding. The presence of AscA had an initial positive effect on binding observed for all three *Nc*LPMOs, but during the next hour the bound fractions of all three LPMOs gradually decreased

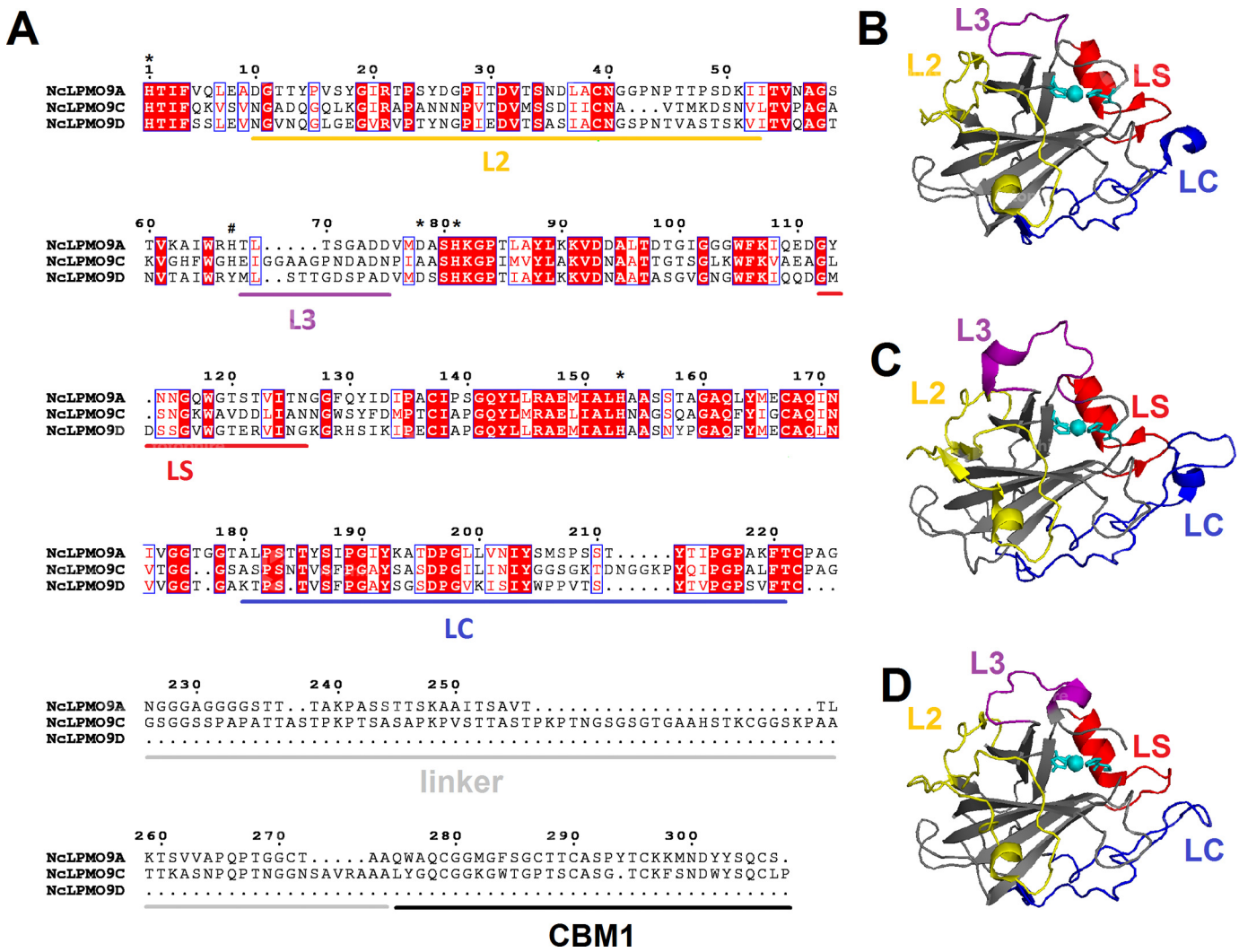

Figure 1. Sequence alignment and structural representation of C4-oxidizing *Nc*LPMOs. *A*, sequence alignment of *Nc*LPMO9A, *Nc*LPMO9C, and *Nc*LPMO9D with fully conserved residues shown in *white* (on a *red background*). The sequence numbering refers to *Nc*LPMO9A. *Blue frames* indicate residues with similar physicochemical properties (printed in *red* on a *white background*). The loop regions that potentially contribute to functional variation among LPMOs, named L2, L3, LS, and LC, are marked with *yellow*, *purple*, *red*, and *blue horizontal bars*, respectively. Family 1 carbohydrate-binding modules and linkers are marked by *black* and *gray horizontal bars*, respectively. *Asterisks* indicate amino acid residues whose amide NMR signals shift upon binding to oligocellulose or xyloglucan (*i.e.* every tested substrate so far) to *Nc*LPMO9C (46); these include His-1 and His-81, which make up the histidine brace. The *hashtag* indicates a histidine residue in a surface loop that includes the L3 region, which NMR studies showed is involved in binding of xyloglucan. *B–D*, cartoon representation of the catalytic domain structures of *Nc*LPMO9A (*B*), *Nc*LPMO9C (*C*), and *Nc*LPMO9D (*D*) with copper depicted as a *cyan sphere* and L2, L3, LS, and LC loops colored in *yellow*, *purple*, *red*, and *blue*, respectively.

(Fig. 3*B*). When equilibrium was reached, the fractions of bound protein were lower than those in the reactions without AscA. Analysis of the experiments shown in Fig. 3 by SDS-PAGE of nonbound protein showed similar trends (Fig. S1).

Substrate specificity

It has previously been shown that *Nc*LPMO9A and -9D are active on PASC (38), whereas a broader substrate specificity has been demonstrated for *Nc*LPMO9C, which acts on cellooligosaccharides with degree of polymerization ≥5, xyloglucan, glucomannan, and β-glucan (25, 42). To gain further information about substrate specificity of each of the three *Nc*LPMOs, their activities were tested in the presence of AscA and single hemicelluloses but also on more complex substrates whereby PASC was premixed with different hemicelluloses. Product mixtures were analyzed by high-performance anion-exchange chromatography with pulsed amperometric detection (HPAEC-PAD) and MALDI-TOF MS.

When using PASC as a substrate, HPAEC-PAD analysis showed, as expected, only products oxidized at the C4 position for all three LPMOs (Fig. S2). Considerable amounts of native products were also detected, which is due in part to on-column conversion of C4-oxidized cellodextrins to native compound with one less sugar (the oxidized sugar is chemically removed (48)). Of note, native species emerge when LPMOs act close to chain ends of cellulose, which is more pronounced on amorphous substrates (44). In this case, the ratio of native-to-oxidized species is relatively high at low conversion levels as visible in Fig. S2.

Activity on tamarind xyloglucan (TXG) was detected for *Nc*LPMO9C and *Nc*LPMO9D but not for *Nc*LPMO9A. The product profile generated by *Nc*LPMO9C was as reported pre-

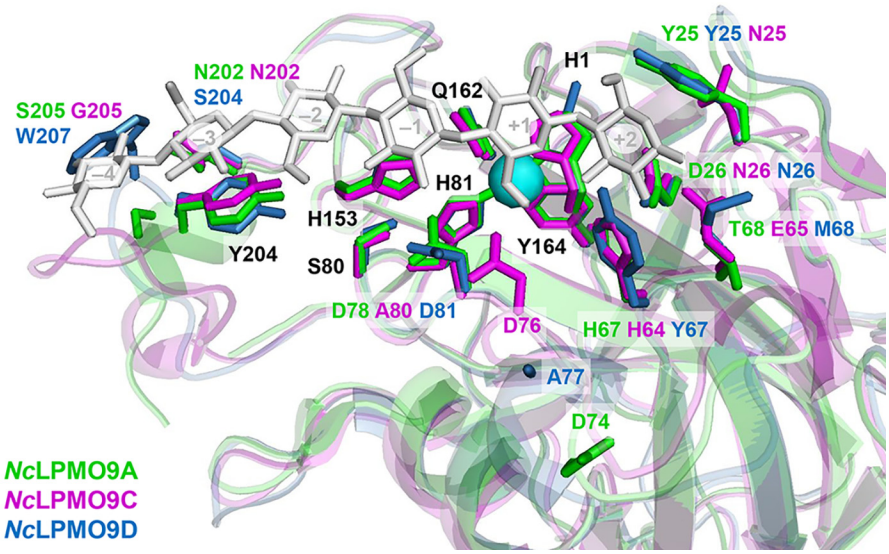

Figure 2. Amino acids potentially involved in substrate binding in *Nc*LPMO9A (*green*), *Nc*LPMO9C (*magenta*), and *Nc*LPMO9D (*blue*). Substrate binding was predicted based on superposition of the crystal structures of *Nc*LPMO9A (PDB code 5FOH; this study), *Nc*LPMO9C (PDB code 4D7U (39)), and *Nc*LPMO9D (PDB code 4EIR (37)) with *Ls*AA9A in complex with cellohexaose (PDB code 5ACI (47)); the picture shows the side chains of the three *Nc*LPMO9s. Amino acids are numbered based on *Nc*LPMO9A (see Fig. 1*A*). Fully conserved residues have *black* labels, whereas not fully conserved residues have multiple labels that are colored according to the corresponding LPMO. The *numbers* within the sugar units (shown in *light gray*) indicate subsites. For clarity, the catalytic copper of only *Nc*LPMO9A and only one of the conformations for the side chains of the residues Tyr-25 and Ala-77 in *Nc*LPMO9D are shown.

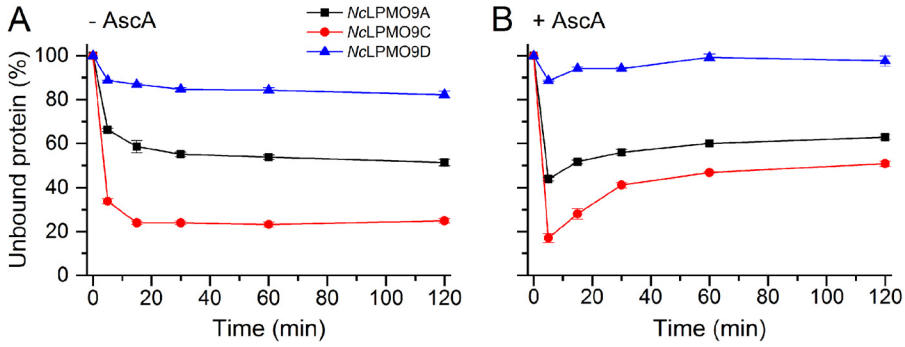

Figure 3. Time-dependent binding of C4-oxidizing *Nc*LPMOs to PASC in the absence (*A*) and presence (*B*) of 1 mM AscA. The percentage of unbound LPMO was determined by measuring the reduction in the concentration of LPMO in solution over time. The experiments were carried out using 2 mg·ml^{-1} PASC and 5 μM LPMO in 50 mM Bis-Tris (pH 6.5) at 45 °C and 1000 rpm. *Error bars* represent S.D. of triplicate samples. Analysis of the same experiments by SDS-PAGE showed similar trends (Fig. S1).

viously (25). *Nc*LPMO9D yielded less intense peaks (Fig. S3*A*), indicating weaker activity of this LPMO on TXG or possibly reflecting that this LPMO is rapidly inactivated in reactions with TXG. MALDI-TOF MS spectra confirmed the TXG activity of *Nc*LPMO9C and *Nc*LPMO9D, showing characteristic clusters of products where each cluster contains products where the number of pentoses equals a multitude of 3 (Fig. 4*A*). According to the MS data, the products released by *Nc*LPMO9C and *Nc*LPMO9D were identical (Fig. 4*B*), and the clustered product profiles indicate that for both LPMOs the lytic reaction occurs at the nonsubstituted glucosyl unit.

Remarkably, when incubating *Nc*LPMO9A with a mixture of TXG and PASC, this LPMO showed activity on TXG, yielding products similar to the other two LPMOs (Figs. 4, *C* and *D*, and S3*B*). Although quantitative interpretation of MS data requires caution, it is worth noting the differences between the LPMOs that are visible in Fig. 4*D*: whereas the product spectrum for *Nc*LPMO9C almost exclusively shows xyloglucan-derived products, the product spectra of the other two show considerable amounts of PASC-derived products.

HPAEC-PAD chromatograms showed that all three LPMOs generated were active on konjac glucomannan (KGM), with *Nc*LPMO9D being the least efficient (Fig. 5*A*). Analysis of the reaction products by MALDI-TOF MS confirmed oxidative activity on KGM, as oxidized hexose oligomers as well as their acetylated and double acetylated forms (characteristic for KGM) appeared in the spectra (Fig. S4). HPAEC-PAD chromatograms further showed that the activity on KGM was promoted by the presence of PASC, in particular for *Nc*LPMO9D (compare Fig. 5, *A* and *B*).

Activity on cellopentaose was confirmed only for *Nc*LPMO9C as reported before (42), whereas only trace activities were detected for both *Nc*LPMO9A and *Nc*LPMO9D (Fig. S5). No activity for any LPMO was observed toward birchwood xylan and ivory nut mannan, either in the absence or in the presence of PASC (data not shown). In the absence

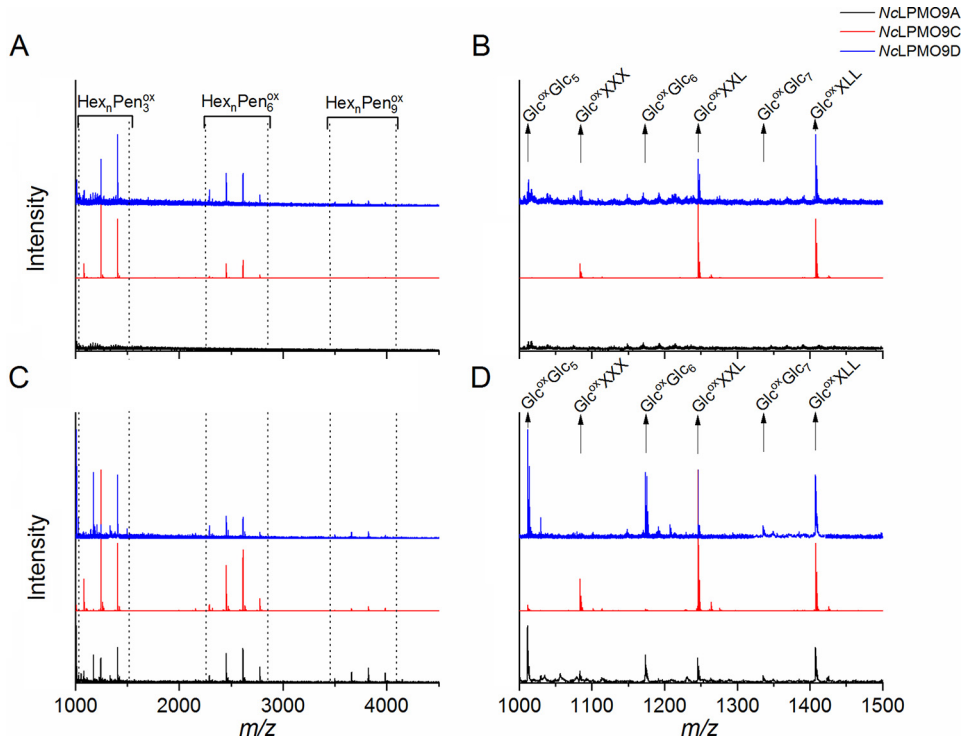

Figure 4. Reaction products generated from TXG and from TXG coated on PASC. The figures show MALDI-TOF MS spectra of products generated from TXG (*A*) with a close-up of the $Hex_nPen_3^{ox}$ region (*B*) or TXG coated on PASC (*C*) with a close-up of the $Hex_nPen_3^{ox}$ region (*D*) by *Nc*LPMO9A (*black*), *Nc*LPMO9C (*red*), and *Nc*LPMO9D (*blue*). Due to the substitution pattern of TXG, where blocks of three substituted glucose units are interspersed with one nonsubstituted glucose, the products appear in clusters where in each cluster the number of pentoses equals a multitude of 3. Variation in the number of hexoses is due to further substitution of the xyloses. Abbreviations (for details see Refs. 25 and 79) used are: *Hex*, hexose (+162 Da); *Pen*, pentose (+132 Da); *Glc*, glucose; *X*, α-D-Xyl-(1→6)-β-D-Glc; *L*, β-D-Gal-(1→2)-α-D-Xyl-(1→6)-β-D-Glc; *ox*, oxidized. Note that in product spectra generated from TXG (*B*), only products characteristic for xyloglucan appear: $Glc^{ox}XXX$, $Glc^{ox}XXL$, and $Glc^{ox}XLL$. Product spectra generated from TXG coated on PASC (*D*) also show oxidized products derived from cellulose: $Glc^{ox}(Glc)_5$, $Glc^{ox}(Glc)_6$, and $Glc^{ox}(Glc)_7$.

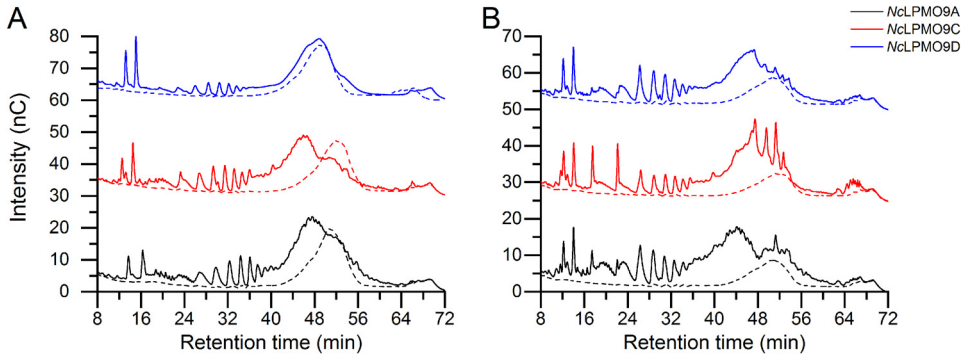

Figure 5. HPAEC-PAD profiles of soluble reaction products generated by C4-oxidizing *Nc*LPMOs from KGM (*A*) and KGM coated on PASC (*B*). Reaction mixtures contained 1 μM *Nc*LPMO9A (*black*), 1 μM *Nc*LPMO9C (*red*), or 1 μM *Nc*LPMO9D (*blue*) and 2 mg·ml^{-1} KGM (*A*) or 2 mg·ml^{-1} KGM and 2 mg·ml^{-1} PASC (*B*) with (*solid lines*) or without (*dashed lines*) AscA. Note that the LPMO activity not only leads to generation of KGM-derived products eluting between 24 and 40 min but also to a shift of the broad substrate peak that is visible in the control reactions without AscA. Peaks eluting prior to 24 min include oxidized AscA and, in *B*, oxidized cello-oligomers.

of an electron donor, no activity was detected for any substrate.

Variation of electron donors

The dependence of the activity of the *Nc*LPMOs on the nature of the reductant was tested in the reactions with PASC using AscA as a nonenzymatic electron donor and cellobiose dehydrogenase from *Myriococcum thermophilum* (*Mt*CDH) or pyrroloquinoline quinone (PQQ)-dependent pyranose dehydrogenase from *Coprinopsis cinerea* (*Cc*PDH) as enzymatic electron donors.

Fig. 6 shows clear dose-response effects upon varying the concentration of AscA. Of note, in these reactions one molecule of AscA is expected to be consumed per substrate oxidation, and the amount of substrate oxidations may be underestimated, likely by a factor of approximately 2 (49), because only solubilized products are detected. In the reactions with 0.3 mM AscA, the maximum amount of released oxidized product was similar for all three LPMOs and in the order of 100 μM (Fig. 6*A*). In this case, the observed termination of product formation is likely due to depletion of the reductant. Higher concentrations of reductant (Fig. 6, *B–D*) gave faster initial rates and higher

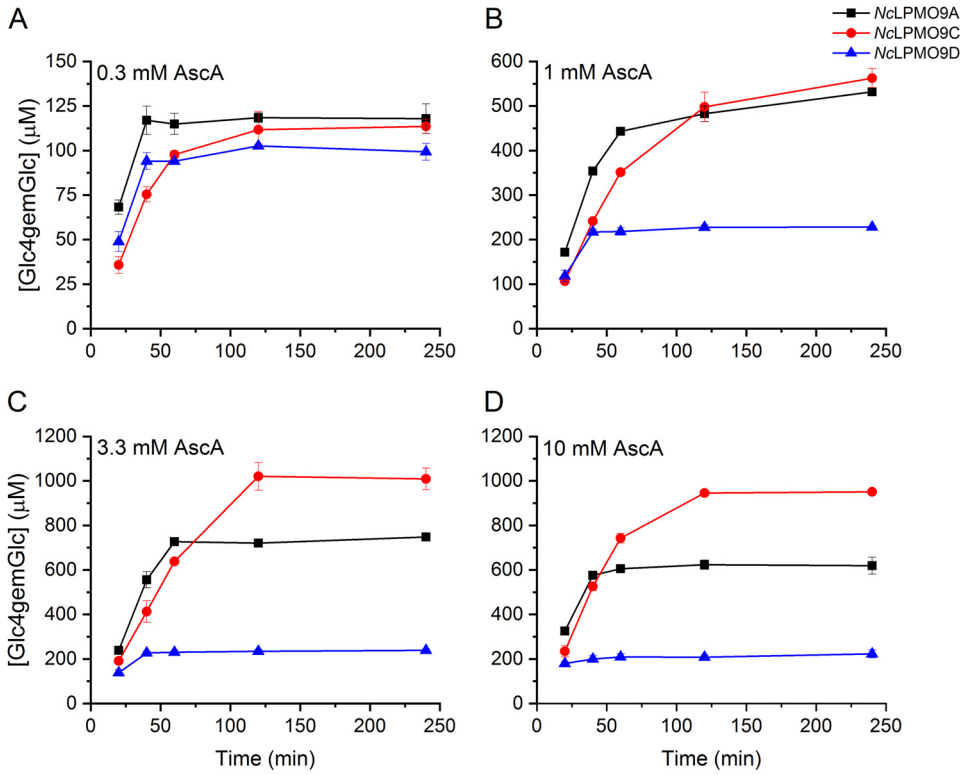

Figure 6. Time course for release of oxidized products during incubation of 1 μM *Nc*LPMO with 2 mg·ml^{-1} PASC and 0.3 (*A*), 1 (*B*), 3.3 (*C*), or 10 mM (*D*) AscA. *Nc*LPMO9A (*black*), *Nc*LPMO9C (*red*), and *Nc*LPMO9D were incubated with PASC and different concentrations of AscA in 50 mM Bis-Tris (pH 6.5) at 45 °C and 1000 rpm. Solubilized oxidized products were enzymatically converted to Glc4gemGlc using 1 μM *Tr*Cel7A. The concentrations of Glc4gemGlc were determined by HPAEC-PAD using a Glc4gemGlc standard prepared as described previously (22). *Error bars* represent S.D. of triplicate samples.

total yields of oxidized products but also increased enzyme inactivation. The latter is suggested by the fact that product formation stopped at product concentrations far below the concentration of AscA (*e.g.* at 0.6 mM in the reaction with *Nc*LPMO9A and 10 mM AscA). Control experiments in which the reactions with 3.3 mM AscA were supplied with all possible combinations of fresh AscA, PASC, and/or LPMO after 240 min (*i.e.* at the end points shown in Fig. 6*C*) showed that only additions containing fresh enzyme led to restoration of product formation (Fig. S6). This confirms that the cessation of product formation indeed is due to enzyme inactivation. In terms of inactivation, the three LPMOs showed clear differences (Fig. 6): although *Nc*LPMO9D became rapidly inactivated and yielded low product levels, *Nc*LPMO9A and, even more so, *Nc*LPMO9C were less sensitive to increased AscA levels, stayed active for a longer time, and reached higher product levels.

*Mt*CDH is known to be able to oxidize oligocellulose and cellulose, whereas the PQQ-dependent *Cc*PDH preferably oxidizes monosaccharides with a $^1C_4$ chair conformation such as L-fucose and D-arabinose (50, 51). Therefore, the reactions with *Cc*PDH were fueled by addition of 1 mM L-fucose. Due to the ability of *Mt*CDH to oxidize products released upon LPMO action on PASC, in the reactions with this electron donor it was not possible to calculate the concentration of products oxidized by LPMOs themselves. We could only assess the amount of C1-oxidized sites, which again reflects the degree of substrate solubilization by the LPMO.

Product formation in reactions with these enzymatic donors (Fig. 7) was remarkably different from the results obtained with AscA (Fig. 6). In all cases, more or less linear progress curves were obtained, and the enzyme performing best with AscA, *Nc*LPMO9C, was clearly the least active in the reactions with *Mt*CDH or *Cc*PDH (Fig. 7). *Nc*LPMO9D performed very well, and the reaction with *Cc*PDH yielded product levels higher than in any of the AscA reactions without showing signs of enzyme inactivation. A control experiment using the conditions of Fig. 6*C* showed that the activity of *Nc*LPMO9D was not improved by addition of 0.5 μM BSA (data not shown), indicating that the good performance of this enzyme in the presence of enzymatic electron donors is not due to the mere presence of additional protein. *Nc*LPMO9A performed well with both AscA and the enzymatic electron donors.

H_2O_2 production

Reduced LPMOs can carry out an oxidase reaction leading to the production of H_2O_2 (36, 42), which is a cosubstrate for LPMOs (35). It has been suggested that generation of H_2O_2 may be rate-limiting in most "standard" LPMO reactions (O_2 and *e.g.* AscA) (11, 35), but this remains somewhat controversial (52). We tested the ability of the three *Nc*LPMO9s to produce H_2O_2 in the presence of 50 μM AscA as reductant and absence of substrate. The measured initial H_2O_2 production rates were 1.13 ± 0.05, 0.60 ± 0.08, and 0.91 ± 0.02 min^{-1} for *Nc*LPMO9A, *Nc*LPMO9C, and *Nc*LPMO9D, respectively (Fig. S7). It is worth noting that these rates are in the same order as

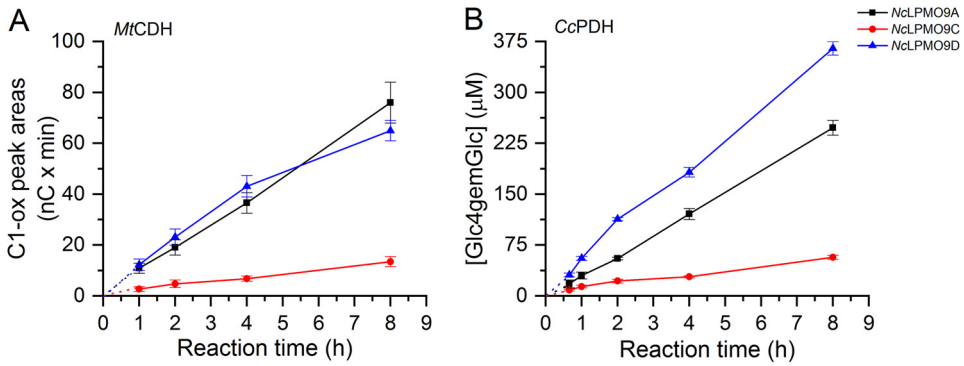

Figure 7. Time course for release of oxidized products during incubation of 1 μM *Nc*LPMO with 2 mg·ml^{-1} PASC and 0.5 μM *Mt*CDH (*A*) or 0.5 μM *Cc*PDH (*B*). *Nc*LPMO9A (*black*), *Nc*LPMO9C (*red*), and *Nc*LPMO9D (*blue*) were incubated with PASC and *Mt*CDH or *Cc*PDH in 50 mM Bis-Tris (pH 6.5) at 45 °C and 1000 rpm. In the reactions with *Mt*CDH, the amount of released soluble products is expressed as the sum of the integrated peak areas (nC × min) for C1-oxidized (*C1-ox*) products only (in this case, C4-oxidized products cannot be detected as they are oxidized at C1 position by CDH). In the reactions with *Cc*PDH, the released oxidized products for each sample were enzymatically converted to Glc4gemGlc using 1 μM *Tr*Cel7A. The concentrations of Glc4gemGlc in every sample were then determined by HPAEC-PAD using Glc4gemGlc standard prepared as described previously (22). Consequently, values on the *y axis* in *A* and *B* should not be compared; quantitative assessment is only valid for comparing the *Nc*LPMOs within the same panel. Results from the reactions with *Cc*PDH may be compared with the results obtained in the reactions with different AscA concentrations (Fig. 6). *Error bars* represent S.D. of triplicate samples.

initial catalytic rates that could be estimated from the reactions with 0.3 mM AscA (Fig. 6*A*) and that the ranking of the LPMOs in terms of speed is the same.

H_2O_2-driven substrate degradation

Next, we assessed whether reactions with the three LPMOs could be fueled by H_2O_2. To do so, reaction mixtures were fed with low amounts of AscA, to secure reduction of the LPMO, and low amounts of H_2O_2 that were low enough to prevent enzyme inactivation. In the control reactions, only AscA was added, in the same concentrations as in the reactions with H_2O_2.

HPAEC and MALDI-TOF MS analyses of generated products (Figs. 8, S8, and S9) did not reveal any differences compared with the reactions performed with 1 mM AscA and no added H_2O_2 (see Fig. S10 for a direct comparison). In the reactions with PASC, only C4-oxidized products were detected, and, as observed above, *Nc*LPMO9D released slightly longer products compared with *Nc*LPMO9A and *Nc*LPMO9C (Fig. 8*A*). Reactions without added H_2O_2 gave almost no products, as one would expect at these very low AscA concentrations (see dose-response curve for AscA in Fig. 6). Likewise, reactions with TXG (Fig. 8*B*) gave the same results as the reactions with high AscA discussed above (Fig. S3*A*): *Nc*LPMO9C showed high activity toward TXG, whereas *Nc*LPMO9D showed less activity, and *Nc*LPMO9A seemed inactive. As above, when TXG was premixed with PASC (Fig. 4, *C–D*), *Nc*LPMO9A showed activity on TXG in the H_2O_2-fueled reaction (Fig. S8). MS data showed that for all three LPMOs the cleavage pattern of TXG was the same in O_2- and H_2O_2-fueled reactions (Figs. 8*D* and S8 *versus* Fig. 4). The results of H_2O_2-fueled reactions with KGM were also very similar to the results obtained under standard conditions (1 mM AscA and no added H_2O_2; Fig. 5): *Nc*LPMO9A and -9C showed high activity, whereas the activity of *Nc*LPMO9D on this substrate was barely detectable unless PASC was also present (Fig. S9, *A* and *B*). MS analysis showed similar product profiles (Fig. S9, *C* and *D*) as in the reactions with high AscA and no added H_2O_2 (Fig. S4).

Product release during the H_2O_2-driven degradation of PASC

Fig. 9 shows that under the conditions used above, *i.e.* gradual addition of H_2O_2, product formation from PASC was similar for all three LPMOs, suggesting that the amount of added H_2O_2 was limiting product formation under these reaction conditions. *Nc*LPMO9A and -9C showed a linear progress curve throughout the reaction, whereas *Nc*LPMO9D showed signs of inactivation after 3 h, in accordance with the apparent lower operational stability of this enzyme that was also observed in *e.g.* the dose-response study with AscA (Fig. 6). In the linear phase of the reactions, the ratio between the amount of oxidized products and the cumulative amount of added H_2O_2 was between 40 and 60%, which is compatible with close to stoichiometric incorporation of H_2O_2 in oxidized products because some 50% of oxidized sites likely remain in the insoluble material (49).

Discussion

N. crassa is a well-known model organism that also happens to be a proficient plant cell-wall degrader (3). It contains a large arsenal of different CAZymes involved in plant biomass degradation. Annotation of the genome shows that family AA9 LPMOs have the highest multiplicity of all CAZymes in *N. crassa*, with 14 genes predicted to encode such enzymes (6). For nine of these 14 LPMO9s, activity on cellulose has been demonstrated, and three of these (*Nc*LPMO9A, -9C, and -9D) are strict C4 oxidizers. As structural comparisons and sequence alignments alone cannot provide a biological rationale for the multiplicity of *lpmo9* genes, such as different roles during plant cell wall degradation, we carried out functional comparison of the three C4-oxidizing *Nc*LPMOs.

Binding of LPMOs to their substrates may be enhanced by CBMs as in other fungal plant cell wall–degrading enzymes. LPMOs with reduced active-site copper and not bound to a substrate are prone to autocatalytic inactivation through nonproductive reactions with O_2 or H_2O_2 (35), and it has indeed been shown that removal of the CBM not only reduces substrate affinity but also LPMO stability (49, 53). Accordingly, the present results show that stability of the three *Nc*LPMO9s cor-

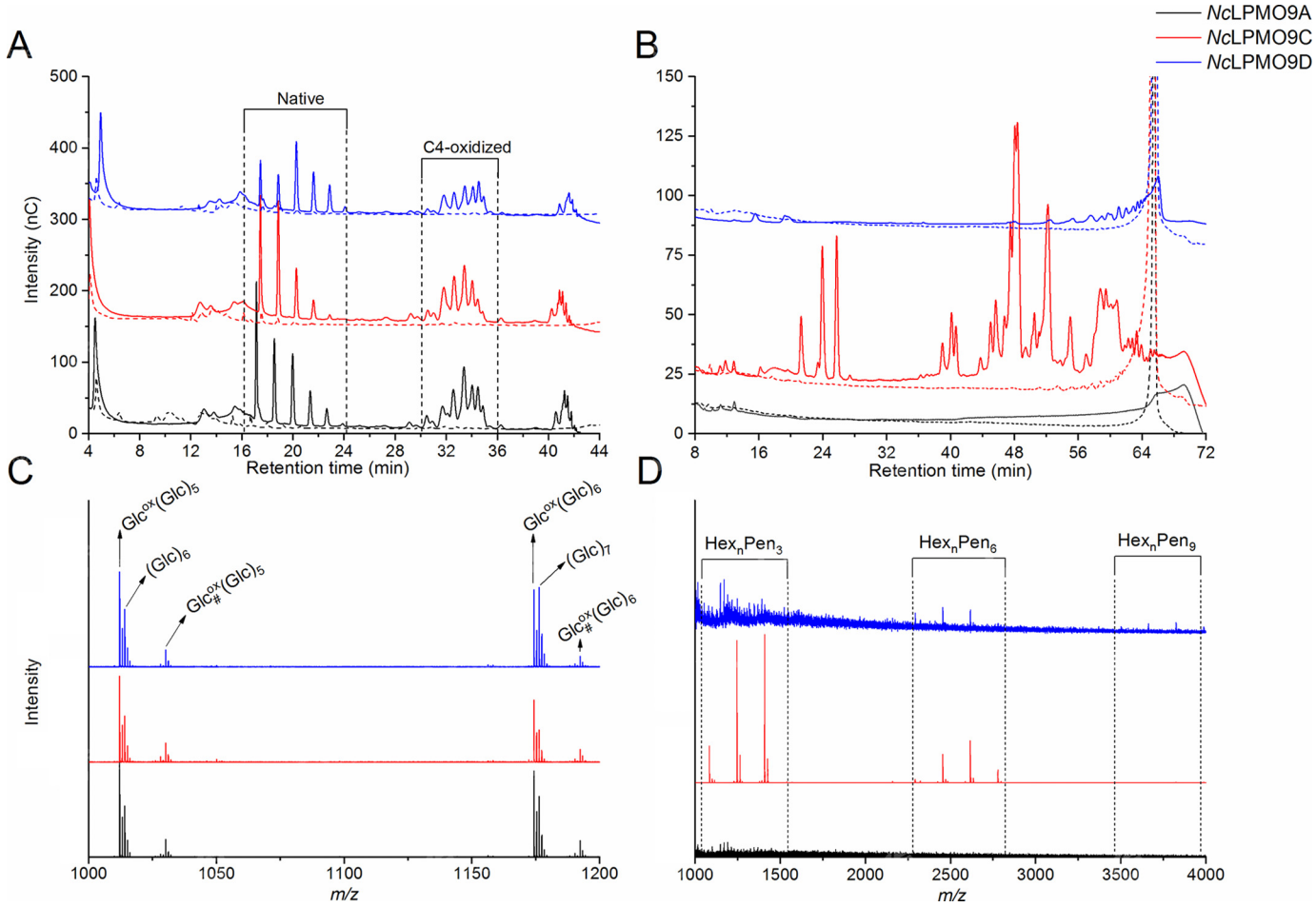

Figure 8. Reaction products generated by C4-oxidizing *Nc*LPMOs from PASC or TXG in reactions with H_2O_2 as a cosubstrate. *A* and *B*, HPAEC-PAD analyses of products generated by 1 μM *Nc*LPMO9A (*black line*), 1 μM *Nc*LPMO9C (*red line*), or 1 μM *Nc*LPMO9D (*blue line*) in reactions with 2 mg·ml^{-1} PASC (*A*) or 2 mg·ml^{-1} TXG (*B*) in 50 mM Bis-Tris (pH 6.5) at 45 °C and 1000 rpm with addition of ~45 μM H_2O_2 to the reactions every 15 min for 4 h. Prior to every addition of H_2O_2, ~12 μM AscA was added to ensure reduction of the LPMO. Control reactions (*dashed lines*) were done in the absence of H_2O_2, meaning that only ~12 μM AscA was added every 15 min for 4 h. The labeling of oxidized cello-oligosaccharides in *A* is based on previous work (42); the identity of the peaks in *B* is unknown due to lack of standards (but see Ref. 25 for some indications). *C*, MALDI-TOF MS spectra of oligosaccharides with DP6 and DP7 released from PASC by *Nc*LPMO9A (*black line*), *Nc*LPMO9C (*red line*), or *Nc*LPMO9D (*blue line*). Peaks representing sodium adducts in the DP6 cluster are labeled, and this cluster shows the native product, $(Glc)_6$ and the oxidized hexamer in its keto form, $Glc^{ox}(Glc)_5$, and in its *gem*-diol form, $Glc_{\#}{}^{ox}(Glc)_5$. *D*, MALDI-TOF MS spectra of products generated from TXG by *Nc*LPMO9A (*black*), *Nc*LPMO9C (*red*), and *Nc*LPMO9D (*blue*). Clusters of products where the number of pentoses equals a multitude of 3 are indicated.

relates with substrate affinity. *Nc*LPMO9D, without a CBM1 and showing the weakest substrate binding, became rapidly inactivated, yielded low product levels, and was more sensitive to even low AscA levels than *Nc*LPMO9A and *Nc*LPMO9C (both containing a CBM1). In contrast, *Nc*LPMO9C, showing the strongest substrate binding, was the most stable of the three LPMOs. The high operational stability observed for *Nc*LPMO9C under standard conditions (high AscA with O_2) may also be due to a lower rate of H_2O_2 production (Fig. S7), which could reduce the chance of potentially destructive encounters of nonsubstrate-bound LPMO and H_2O_2. It is noteworthy that the considerable differences in substrate binding between the three LPMOs are not reflected in major differences in the initial catalytic rates, indicating the importance of other factors, such as enzyme mobility on the substrate surface, in enzyme catalysis.

Our results confirm previous observations that reduction of the active-site copper promotes substrate binding (43, 46). The gradual decrease in substrate binding over time, which is visible in Figs. 3 and S1, likely reflects oxidative damage of the LPMO catalytic site and not just reoxidation of the copper, as over time the bound fraction of LPMOs in the presence of AscA was less than in the reactions without AscA.

Importantly, in-depth functional characterization of the three C4-oxidizing *Nc*LPMO9s revealed clear differences in substrate preferences. Only *Nc*LPMO9C is active on shorter cello-oligosaccharides, whereas only *Nc*LPMO9C and *Nc*LPMO9D are active on TXG. Interestingly, *Nc*LPMO9A did show activity on TXG in reactions that also contained cellulose. It is likely that hemicelluloses such as TXG associate with cellulose (54–56), creating junction zones between cellulose and hemicelluloses that enable the LPMO to act also on the now "stabilized" hemicellulose (see also Ref. 30). Further illustrating differences between the LPMOs, in reactions with PASC–TXG mixtures, PASC was still the preferred substrate for *Nc*LPMO9A and *Nc*LPMO9D, whereas *Nc*LPMO9C primarily acted on TXG. Addition of cellulose also promoted activity of the LPMOs on KGM, in particular for *Nc*LPMO9D, which was hardly active on KGM alone. It is worth noting that in

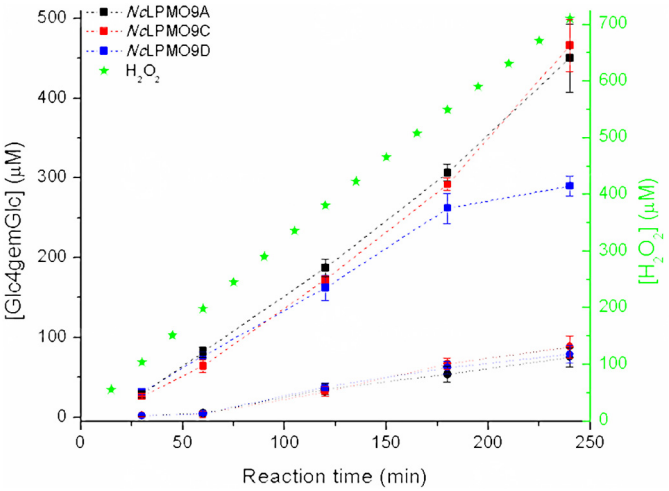

Figure 9. Time course for release of oxidized products during incubation of 2 mg·ml^{-1} PASC with 1 μM C4-oxidizing *Nc*LPMO in reactions with H_2O_2 (*dashed lines*). *Nc*LPMO9A (*black squares*), *Nc*LPMO9C (*red squares*), and *Nc*LPMO9D (*blue squares*) were incubated with 2 mg·ml^{-1} PASC in 50 mM Bis-Tris (pH 6.5) at 45 °C and 1000 rpm, and ~45 μM H_2O_2 was added to the reactions every 15 min. Prior to every addition of H_2O_2, ~12 μM AscA was added to ensure reduction of the LPMO. Control reactions (●, connected with *dotted lines*) were done in the absence of H_2O_2, meaning that only ~12 μM AscA was added every 15 min for 4 h. Solubilized oxidized products were enzymatically converted to Glc4gemGlc using 1 μM *Tr*Cel7A. The concentrations of Glc4gemGlc, shown on the *left y axis*, were determined by HPAEC-PAD using a Glc4gemGlc standard prepared as described previously (22). *Error bars* represent S.D. of triplicate samples. Note that only soluble oxidized products were measured and that the nonsoluble material contains a significant fraction of the oxidized sites. The cumulative amount of H_2O_2 that was added to the reactions is indicated by *green asterisks*, and the concentration values are shown on the *right y axis*.

reactions with TXG the effect of adding cellulose was largest for *Nc*LPMO9A, whereas it was largest for *Nc*LPMO9D in reactions with KGM. Although further studies on true copolymeric substrates, such as intact plant cell walls, are needed, the present findings clearly show that the three seemingly similar *Nc*LPMO9s have different substrate specificities that may relate to the complex structure of the plant cell wall.

Structural comparisons do not provide obvious explanations for the differences in substrate specificity. In accordance with previous studies on the binding of polymeric substrates (13, 46, 57), it may seem that a larger part of the putative substrate-binding surface is involved in determining substrate preferences. It is known that the L3 region is involved in binding xyloglucan, and Figs. 1 and 2 show that the three LPMOs exhibit relatively much variation in this region, affecting *e.g.* subsite +2. It is worth noting that the LPMO without a CBM, *Nc*LPMO9D, contains relatively many aromatic residues near the substrate-binding surface (Tyr at positions 25 and 67, subsite +2; Trp at position 205, subsite −4; see Fig. 1*A*) that may add to substrate affinity and could thus, perhaps, compensate for the lack of a CBM. However, mutagenesis studies on the proposed residues will need to be performed before conclusions on the role of these residues in substrate binding can be drawn.

It has previously been shown that LPMOs differ when it comes to their interactions with small-molecule reductants (58, 59). Here, we analyzed both a small-molecule reductant, AscA, and two enzymatic electron donors, *Mt*CDH and *Cc*PDH. The three LPMOs showed remarkable differences in operational stability and ability to recruit electrons from these varying electron donors. Slower, controlled activation of the LPMOs with an enzymatic donor increased the operational stability of *Nc*LPMO9D, whereas AscA was the better electron donor for *Nc*LPMO9C. Interestingly, in the reactions with enzymatic electron donors, the efficiency of the LPMOs was very different from that in reactions with AscA and inversely correlated to the LPMOs' ability to bind substrate. For *Nc*LPMO9C, it has been shown that the presence of substrate reduces the ability of CDH to reduce the LPMO (46), which could explain why tight substrate binders are less easily reduced by an enzymatic electron donor. In line with this, Várnai *et al.* (60) have shown that difference in the activation of different LPMOs by *Cc*PDH can be abolished by addition of a small redox mediator, which can more easily access the active site of an LPMO bound to a substrate. The operational stability of the LPMO in the presence of various reductants is determined in part by the extent to which the LPMO is close to the substrate as it becomes reduced. The results with *Nc*LPMO9D seem to support the notion that LPMO reduction close to the substrate is favorable: this LPMO, showing weak substrate binding and low operational stability when reduced by AscA, fully maintained operational stability when fueled by the CBM-containing and thus likely substrate-bound *Cc*PDH.

The results presented above lend further support to the recent claims that H_2O_2 is a preferred, if not the only, cosubstrate of LPMOs (34, 35). All three *Nc*LPMO9s could efficiently use added H_2O_2 as a cosubstrate, whereas their activity under standard conditions (1 mM AscA with no added H_2O_2) was correlated with their ability to produce H_2O_2. It has been proposed that H_2O_2-driven LPMO reactions are less specific than O_2-driven reactions because oxidative damage in the LPMO, claimed to only occur in the H_2O_2-driven reaction, would compromise enzyme specificity (52). Although reduction of specificity due to oxidative damage in the active site certainly is conceivable, we would argue that this possible process is not related to the nature of the cosubstrate used. Rather, the degree of oxidative damage, for example caused by a surplus of H_2O_2 reacting with nonsubstrate-bound reduced LPMOs, is due to an imbalance between the various reactants that leads to nonproductive and potentially damaging LPMO reactions. Here, we show that in well-controlled reactions O_2- and H_2O_2-fueled reactions yield essentially identical product profiles for all three LPMOs with PASC, xyloglucan, and glucomannan. Fig. 9 shows that under controlled conditions one may achieve stoichiometric incorporation of H_2O_2, whereas the enzymes show good stability. These results show that the specificity of the LPMO is independent of the nature of the cosubstrate used to drive the reaction.

All in all, the present study shows that the three C4-oxidizing cellulose-active LPMOs of *N. crassa* exhibit a variety of functional differences that may relate to their biological roles. Most importantly, although the true natural substrates of these LPMOs, such as, possibly, certain substructures of the plant cell wall, still need to be discovered, our results clearly show that the three enzymes have different substrate specificities. Another major difference concerns the interplay

with varying reductants, which is interesting because the availability of both enzymatic and nonenzymatic electron donors will vary during plant cell wall degradation both in space and time (9, 61). Thus, it is conceivable that these three LPMOs have distinctive roles during degradation of the complex cell wall, which could explain the multiplicity of LPMOs in plant cell wall–degrading fungi.

Experimental procedures

Chemicals

Bis-Tris buffer salt was purchased from VWR (Radnor, PA); hydrogen peroxide (30% aqueous solution) was purchased from Merck; ascorbic acid, L-fucose, Avicel® PH-101, xylan from birch wood, horseradish peroxidase, and 10-acetyl-3,7-dihydroxyphenoxazine (AmplexRed) were purchased from Sigma-Aldrich. Cellopentaose (purity >95%), xyloglucan from tamarind seeds (purity ~95%), konjac glucomannan (purity >98%), and ivory nut mannan (purity >98%) were purchased from Megazyme (Bray, Ireland). PASC was prepared from Avicel PH-101 as described before (62).

Enzymes

*Mt*CDH and PQQ-dependent *Cc*PDH were expressed in *Pichia pastoris* and purified as reported previously (63, 64). The enzyme concentrations of *Mt*CDH and *Cc*PDH preparations were determined by measuring absorbance at 280 nm and using molar extinction coefficients of 159,000 and 146,500 $M^{-1}\cdot cm^{-1}$, respectively, determined using the ExPASy ProtParam tool (65).

Cloning, expression, and purification of LPMOs from N. crassa

The gene encoding *Nc*LPMO9A with its native signal peptide was codon-optimized for expression in *P. pastoris* and ordered from GenScript (Piscataway, NJ) in a pUC57 vector. A Kozak sequence (GAAACG) was inserted upstream of the start codon, and EcoRI and Acc65I restriction sites were introduced for cloning in the 5′ and 3′ ends, respectively. The pUC57 vector containing the codon-optimized sequence was digested by EcoRI and Acc65I, and the gene fragment was ligated into EcoRI/Acc65I-digested pPINK-GAP_TaCel5A (66), yielding pPINK-GAP_2240. The expression vector was transformed into *Escherichia coli* TOP10 (Invitrogen), and transformants were selected on brain–heart infusion agar with 200 $\mu g\cdot ml^{-1}$ ampicillin. The pPINK-GAP_2240 plasmid was purified, linearized with AflII, and transformed into electrocompetent cells of *P. pastoris* PichiaPink™ Strain 4. Electrocompetent *P. pastoris* cells were prepared by following the manufacturer's procedure. The electrocompetent cells were electroporated using a Bio-Rad Gene Pulser II electroporation unit (Bio-Rad Laboratories) at 1.8 kV, 25 microfarads, 200 ohms. The transformed cells were incubated in yeast extract–peptone–dextrose medium containing 1 M sorbitol overnight and spread on *Pichia* adenine-dropout selection plates, which were incubated at 30 °C.

For purification, the production strain was grown in 20 ml of buffered complex glycerol medium containing 1% (v/v) glycerol in a 100-ml shake flask at 29 °C and 200 rpm for 16 h. Subsequently, this preculture was used to inoculate 0.5 liter of buffered complex glycerol medium containing 1% (v/v) glycerol in a 2-liter shake flask followed by incubation at 29 °C and 200 rpm for 48 h. After 24 h, the culture was supplemented with 1% (v/v) glycerol. The cells were removed by centrifugation at 7,000 × *g* for 15 min at 4 °C. The supernatant was collected and dialyzed against 50 mM Bis-Tris buffer (pH 6.5) and concentrated to 100 ml using a VivaFlow 200 tangential cross-flow concentrator (molecular mass cutoff, 10 kDa; Sartorius Stedim Biotech GmbH, Germany). Ammonium sulfate was added to the concentrated supernatant to a final concentration of 1.42 M after which the solution was loaded onto a 5-ml HiTrap Phenyl FF column (GE Healthcare) equilibrated with 50 mM Bis-Tris buffer (pH 6.5) containing 1.42 M ammonium sulfate. Proteins bound to the column were eluted using a 25-ml linear gradient from 1.42 to 0 M ammonium sulfate in 50 mM Bis-Tris buffer (pH 6.5) using a flow rate of 1 $ml\cdot min^{-1}$. Collected fractions were analyzed by SDS-PAGE, and the fractions containing *Nc*LPMO9A were pooled and subsequently concentrated down to 2 ml using Amicon Ultra centrifugal filters (molecular mass cutoff, 10 kDa; Merck Millipore). The protein solution was loaded onto a HiLoad 16/60 Superdex 75 size-exclusion column (GE Healthcare) in 50 mM Bis-Tris buffer (pH 6.5) containing 150 mM NaCl using a flow rate of 0.75 $ml\cdot min^{-1}$. Fractions containing pure *Nc*LPMO9A were identified using SDS-PAGE and subsequently pooled and concentrated using Amicon Ultra centrifugal filters (molecular mass cutoff, 10 kDa).

*Nc*LPMO9C (UniProt accession number Q7SHI8) was cloned in *P. pastoris* (67) and expressed and purified following a previously published protocol (36). *Nc*LPMO9D (UniProt accession number Q1K8B6) was cloned as described earlier (23) using a protocol similar to that described above for *Nc*LPMO9A and a synthetic gene that encoded the protein with its native signal sequence. The enzyme was purified as described above for *Nc*LPMO9A.

The protein concentrations of *Nc*LPMO9A, *Nc*LPMO9C, and *Nc*LPMO9D preparations were determined by measuring absorbance at 280 nm and using molar extinction coefficients of 45,000, 46,900, and 35,660 $M^{-1}\cdot cm^{-1}$, respectively, determined using the ExPASy ProtParam tool (65). The enzymes were saturated with Cu(II) by incubating with an excess of $Cu(II)SO_4$ (at an ~3:1 molar ratio of copper:enzyme) for 90 min in 50 mM Bis-Tris (pH 6.5) at room temperature as described previously (68). The Cu(II)-loaded sample of *Nc*LPMO9A was buffer-exchanged to 50 mM Bis-Tris buffer (pH 6.5) using Amicon Ultra centrifugal filters (molecular mass cutoff, 3 kDa). The resulting solution with purified protein was filtered through a 0.22-μm Millex®-GV filter (Merck Millipore) and stored at 4 °C.

Crystallization and X-ray data collection

Purified *Nc*LPMO9A was cleaved with papain (papain from papaya latex, Sigma-Aldrich) at an LPMO:papain ratio of 33:1 (w/w) to remove the CBM1 that is appended to the catalytic LPMO9 domain. The reaction was carried out in 100 mM sodium acetate buffer (pH 5.0) for 48 h at 37 °C, and its outcome was assessed by SDS-PAGE. For the isolation of the cleaved

catalytic domain, size-exclusion chromatography was applied using a Superdex 75 16/600 column (GE Healthcare) equilibrated in 50 mM MES (pH 6.5) and 150 mM NaCl. The purified catalytic domain (NCU02240-N) was buffer-exchanged into 20 mM MES (pH 6.5) and concentrated to 15 mg·ml^{-1} for crystallization trials. A wide range of crystallization conditions were tested using a Mosquito crystallization robot (TTP Labtech, UK) and commercially available 96-well kits. Crystals of NCU02240-N grew at room temperature in the presence of 20% PEG3350 and 0.2 M Li_2SO_4 using the sitting-drop vapor-diffusion technique. Before being flash frozen in liquid N_2, a single crystal was cryoprotected by transferring to mother liquor containing 35% PEG3350. X-ray diffraction data were collected to 1.6-Å resolution on beamline ID23-2 (European Synchrotron Radiation Facility, Grenoble, France) under cryogenic conditions. The wavelength of the X-ray beam was 0.8726 Å, and the oscillation range was 0.05°. The resulting data set was processed using XDS (69), and the structure was solved by molecular replacement using Phaser (70). The molecular replacement search model was produced by CHAINSAW (71) using *Nc*LPMO9D (PDB code 4EIR) (37) as the template structure. Iterative rounds of model building and refinement of the structure were performed using Coot (72) and REFMAC (73) from the CCP4i program suite. Solvent molecules were added using Coot and checked manually. The quality of the final structure model was evaluated using MolProbity (74). The final structure model and the structure factors are deposited at the PDB under accession code 5FOH. Data collection and refinement statistics are summarized in Table S1. All structure figures were prepared using the UCSF Chimera package (75).

Binding of LPMOs to PASC

Binding studies with PASC were performed as described before (76) in the presence or absence of 1 mM AscA. The reaction mixtures contained 2 mg·ml^{-1} PASC or 2 mg·ml^{-1} PASC premixed with 1 mM AscA and 5 μM enzyme in 50 mM Bis-Tris buffer (pH 6.5) and were incubated at 45 °C with shaking at 1000 rpm in an Eppendorf ThermoMixer. At various time points (5, 15, 30, 60, and 120 min), samples were taken, and insoluble substrate and substrate-bound enzyme were removed by filtering using a 96-well filter plate (Merck Millipore) operated by a Millipore vacuum manifold. The concentration of the enzyme in the filtrate was determined by measuring A_{280} (Eppendorf BioPhotometer). Furthermore, the filtrates from each time point were mixed with an equal volume of SDS sample buffer and analyzed by SDS-PAGE by loading exactly 5 μl of such prepared samples per well.

LPMO reactions with AscA

Unless otherwise stated, reaction mixtures contained 2 mg·ml^{-1} substrate, 1 μM *Nc*LPMO, and 1 mM AscA in 50 mM Bis-Tris buffer (pH 6.5). Reactions were performed in 2-ml Eppendorf tubes containing 100-μl total reaction volume and incubated at 45 °C with shaking at 1000 rpm in an Eppendorf ThermoMixer. Reactions were stopped by boiling for 10 min. Subsequently, separation of soluble and insoluble fractions was done by centrifugation at 11,000 × *g* for 10 min. As controls, reactions without added reductant were also analyzed.

Detection of oxidized products

Oxidized products were analyzed using HPAEC-PAD and by MALDI-TOF MS. HPAEC was performed on a Dionex ICS5000 system equipped with a CarboPac PA1 analytical column (2 × 250 mm) and a CarboPac PA1 guard column (2 × 50 mm) using a 50-min gradient (44) for cellulosic and a 75-min gradient (25) for hemicellulosic substrates. Chromatograms were recorded with Chromeleon and analyzed using Origin 9.1 software (OriginLab, Northampton, MA).

MALDI-TOF MS was performed on an Ultraflex MALDI-TOF/TOF instrument (Bruker Daltonik GmbH, Bremen, Germany) equipped with a nitrogen 337 nm laser. The instrument was operated in positive-linear acquisition mode. The samples were sodium-saturated by mixing 5 μl of sample with 5 μl of 50 mM sodium acetate. 1 μl of the saturated sample was spotted on an MTP 384 ground steel MALDI target and mixed immediately with an equal volume of 20 mg·ml^{-1} 2,5-dihydroxybenzoic acid in 30% acetonitrile and 0.1% (v/v) TFA. The data were analyzed using mMass software (77). Baseline correction and Gaussian smoothing (window size, 0.3 *m/z*) were applied to all spectra.

Quantitative assessment of products released from PASC with varying electron donors

Reaction mixtures (600 μl) with nonenzymatic electron donors contained 2 mg·ml^{-1} PASC, 1 μM *Nc*LPMO, and 0.33, 1, 3.3, or 10 mM AscA in 50 mM Bis-Tris buffer (pH 6.5). Control reactions to check for substrate, enzyme, and reductant depletion were set up using the same conditions with 3.3 mM AscA in 100 μl; after 240 min, 100 μl of the reaction mixtures were supplemented with 50 μl of buffer (50 mM Bis-Tris (pH 6.5)) or with 50 μl of the same buffer containing various combinations of 2 mg·ml^{-1} substrate, 1 μM LPMO, and 3.3 mM AscA followed by further incubation for 120 min.

Reaction mixtures (600 μl) with an enzymatic electron donor contained 2 mg·ml^{-1} PASC, 1 μM *Nc*LPMO, and 1 μM *Mt*CDH (63) or 1 μM *Cc*PDH (64). The reactions with *Cc*PDH also contained 1 mM L-fucose, acting as a substrate for *Cc*PDH.

All reactions were incubated at 45 °C with shaking at 1000 rpm in an Eppendorf ThermoMixer. At various time points (20, 40, 60, 120, and 240 min), 120-μl samples were taken and boiled for 10 min. Separation of soluble and insoluble fractions was achieved by centrifugation at 11,000 × *g* for 10 min. Prior to product quantification, soluble fractions (32 μl) were mixed with 31 μl of 150 mM sodium acetate buffer (pH 4.5) and 1 μl of *Tr*Cel7A (~1 μM) and incubated for 16 h at 37 °C. The treatment with *Tr*Cel7A converts oligomeric products to a mixture of glucose, cellobiose, and Glc4gemGlc (C4-oxidized cellobiose) as the only oxidized product. Soluble fractions treated in this way were subsequently analyzed using HPAEC-PAD. The amount of released oxidized products was quantified using 4-hydroxy-β-D-xylo-Hex*p*-(1→4)-β-D-Glc*p* (Glc4gemGlc), prepared as described previously (22), as a standard. In the reactions with *Mt*CDH, the sum of integrated peak areas of C1-oxidized products (nC × min) was used as a proxy for LPMO activity.

LPMO reactions with H_2O_2

Unless otherwise stated, reaction mixtures (200 μl) contained 2 mg·ml^{-1} substrate and 1 μM *Nc*LPMO in 50 mM Bis-Tris buffer (pH 6.5). Reactions were initiated by adding 2 μl of 1.5 mM AscA immediately followed by addition of 2 μl of 5 mM H_2O_2. Every 15 min, an additional 2 μl of 1.5 mM AscA and 2 μl of 5 mM H_2O_2 (in this order) were added to the reaction mixtures (15 additions in total over a period of 4 h). Reactions were stopped by boiling for 10 min followed by separation of soluble and insoluble material by centrifugation at 11,000 × *g* for 10 min. Control reactions without added H_2O_2 were also performed.

Quantitative assessment of products released from PASC in reactions with H_2O_2

Reaction mixtures with H_2O_2 (600-μl final volume after initiation of the reaction) contained 2 mg·ml^{-1} PASC and 1 μM *Nc*LPMO in 50 mM Bis-Tris buffer (pH 6.5). Reactions were initiated by adding 6 μl of 1.5 mM AscA (final concentration, 15 μM) followed by addition of 6 μl of 5 mM H_2O_2 (final concentration, 50 μM). After exactly 15 min, an additional 6 μl of 1.5 mM AscA and 5 mM H_2O_2 were added. 30 min after the reactions were initiated, a 122-μl sample was taken from the reaction mixture and boiled for 10 min. To the rest of the reaction mixture (490 μl), 5 μl of 1.5 mM AscA (15 μM) and 5 μl of 5 mM H_2O_2 (50 μM) were added. The same volumes of 1.5 mM AscA and 5 mM H_2O_2 were also added at 45 min after reaction initiation. At 60 min, a 118-μl sample was taken and boiled for 10 min. To the rest of reaction mixture (392 μl), 4 μl of 1.5 mM AscA (15 μM) and 4 μl of 5 mM H_2O_2 (50 μM) were added. The same volumes of 1.5 mM AscA and 5 mM H_2O_2 were also added at 75, 90, and 115 min after the reactions were initiated. After 120 min, 130-μl samples were taken and boiled for 10 min. To the rest of reaction mixture (294 μl), 3 μl of 1.5 mM AscA (15 μM) and 3 μl of 5 mM H_2O_2 (50 μM) were added. The same volumes of 1.5 mM AscA and 5 mM H_2O_2 were added at 135, 150, and 165 min after reaction initiation. After 180 min, 122-μl samples were taken and boiled for 10 min. To the rest of the reaction mixture (196 μl), 2 μl of 1.5 mM AscA (15 μM) and 2 μl of 5 mM H_2O_2 (50 μM) were added, and this was repeated at 195, 210, and 225 min after reaction initiation. After 240 min, the reactions were stopped by boiling for 10 min.

Separation of soluble and insoluble materials was achieved by centrifugation at 11,000 × *g* for 10 min. Samples of the soluble fractions (32 μl) were mixed with 31 μl of 150 mM sodium acetate buffer (pH 4.5) and 1 μl of *Tr*Cel7A (~1 μM) and incubated for 16 h at 37 °C. The oxidized products were subsequently detected and quantified using HPAEC-PAD and Glc4gemGlc as a standard as described above.

H_2O_2 production

Measurement of H_2O_2 production was done as described previously (78). A reaction mixture (180 μl) containing 1 μM LPMO, 5 units·ml^{-1} horseradish peroxidase, and 100 μM AmplexRed in 50 mM Bis-Tris buffer (pH 6.5) was incubated for 5 min at 40 °C in a 96-well microtiter plate in a plate reader (Multiskan^{TM} FC microplate photometer, Thermo Fisher Scientific, Bremen Germany). The reaction was initiated by the addition of 20 μl of 500 μM AscA (50 μM final concentration) in each well, and the production of resorufin was monitored at 540 nm. Control reactions in the absence of LPMO were carried out to obtain the LPMO-independent resorufin production rate. This control reaction provided a background signal equal to 0.3% of the LPMO-catalyzed reaction and was subtracted from the latter. An H_2O_2 standard curve was prepared using the same conditions (without AscA and LPMO). The reactions were monitored for 45 min, and H_2O_2 production rates were derived from data points in the linear region between 0 and 8.5 min.

Author contributions—D. M. P., A. V., M. D., G. M., M. S., B. W., and V. G. H. E. conceptualization; D. M. P., M. D., and M. S. data curation; D. M. P., A. V., and M. D. formal analysis; D. M. P. and M. D. investigation; D. M. P. and A. V. visualization; D. M. P., A. V., and V. G. H. E. writing-original draft; A. V., G. M., M. S., B. W., and V. G. H. E. supervision; M. D., G. M., M. S., B. W., and V. G. H. E. writing-review and editing; M. S. and V. G. H. E. funding acquisition.

References

1. Eberhart, B. M., Beck, R. S., and Goolsby, K. M. (1977) Cellulase of *Neurospora crassa*. *J. Bacteriol.* **130,** 181–186 Medline
2. Yazdi, M. T., Radford, A., Keen, J. N., and Woodward, J. R. (1990) Cellulase production by *Neurospora crassa*: purification and characterization of cellulolytic enzymes. *Enzyme Microb. Technol.* **12,** 120–123 CrossRef Medline
3. Davis, R. H., and Perkins, D. D. (2002) Timeline: *Neurospora*: a model of model microbes. *Nat. Rev. Genet.* **3,** 397–403 CrossRef Medline
4. Martinez, D., Berka, R. M., Henrissat, B., Saloheimo, M., Arvas, M., Baker, S. E., Chapman, J., Chertkov, O., Coutinho, P. M., Cullen, D., Danchin, E. G., Grigoriev, I. V., Harris, P., Jackson, M., Kubicek, C. P., *et al.* (2008) Genome sequencing and analysis of the biomass-degrading fungus *Trichoderma reesei* (syn. *Hypocrea jecorina*). *Nat. Biotechnol.* **26,** 553–560 CrossRef Medline
5. Levasseur, A., Drula, E., Lombard, V., Coutinho, P. M., and Henrissat, B. (2013) Expansion of the enzymatic repertoire of the CAZy database to integrate auxiliary redox enzymes. *Biotechnol. Biofuels* **6,** 41 CrossRef Medline
6. Tian, C., Beeson, W. T., Iavarone, A. T., Sun, J., Marletta, M. A., Cate, J. H., and Glass, N. L. (2009) Systems analysis of plant cell wall degradation by the model filamentous fungus *Neurospora crassa*. *Proc. Natl. Acad. Sci. U.S.A.* **106,** 22157–22162 CrossRef Medline
7. Horn, S. J., Vaaje-Kolstad, G., Westereng, B., and Eijsink, V. (2012) Novel enzymes for the degradation of cellulose. *Biotechnol. Biofuels* **5,** 45 CrossRef Medline
8. Mba Medie, F., Davies, G. J., Drancourt, M., and Henrissat, B. (2012) Genome analyses highlight the different biological roles of cellulases. *Nat. Rev. Microbiol.* **10,** 227–234 CrossRef Medline
9. Kracher, D., Scheiblbrandner, S., Felice, A. K., Breslmayr, E., Preims, M., Ludwicka, K., Haltrich, D., Eijsink, V. G., and Ludwig, R. (2016) Extracellular electron transfer systems fuel cellulose oxidative degradation. *Science* **352,** 1098–1101 CrossRef Medline
10. Lenfant, N., Hainaut, M., Terrapon, N., Drula, E., Lombard, V., and Henrissat, B. (2017) A bioinformatics analysis of 3400 lytic polysaccharide oxidases from family AA9. *Carbohydr. Res.* **448,** 166–174 CrossRef Medline
11. Bissaro, B., Várnai, A., Røhr, Å. K., and Eijsink, V. G. H. (2018) Oxidoreductases and reactive oxygen species in conversion of lignocellulosic biomass. *Microbiol. Mol. Biol. Rev.* **82,** e00029-18 CrossRef Medline
12. Quinlan, R. J., Sweeney, M. D., Lo Leggio, L., Otten, H., Poulsen, J. C., Johansen, K. S., Krogh, K. B., Jørgensen, C. I., Tovborg, M., Anthonsen, A., Tryfona, T., Walter, C. P., Dupree, P., Xu, F., Davies, G. J., *et al.* (2011) Insights into the oxidative degradation of cellulose by a copper metalloen-

zyme that exploits biomass components. *Proc. Natl. Acad. Sci. U.S.A.* **108,** 15079–15084 CrossRef Medline

13. Aachmann, F. L., Sørlie, M., Skjåk-Bræk, G., Eijsink, V. G., and Vaaje-Kolstad, G. (2012) NMR structure of a lytic polysaccharide monooxygenase provides insight into copper binding, protein dynamics, and substrate interactions. *Proc. Natl. Acad. Sci. U.S.A.* **109,** 18779–18784 CrossRef Medline
14. Vaaje-Kolstad, G., Westereng, B., Horn, S. J., Liu, Z., Zhai, H., Sørlie, M., and Eijsink, V. G. (2010) An oxidative enzyme boosting the enzymatic conversion of recalcitrant polysaccharides. *Science* **330,** 219–222 CrossRef Medline
15. Beeson, W. T., Vu, V. V., Span, E. A., Phillips, C. M., and Marletta, M. A. (2015) Cellulose degradation by polysaccharide monooxygenases. *Annu. Rev. Biochem.* **84,** 923–946 CrossRef Medline
16. Hemsworth, G. R., Johnston, E. M., Davies, G. J., and Walton, P. H. (2015) Lytic polysaccharide monooxygenases in biomass conversion. *Trends Biotechnol.* **33,** 747–761 CrossRef Medline
17. Johansen, K. S. (2016) Lytic polysaccharide monooxygenases: the microbial power tool for lignocellulose degradation. *Trends Plant Sci.* **21,** 926–936 CrossRef Medline
18. Vaaje-Kolstad, G., Forsberg, Z., Loose, J. S., Bissaro, B., and Eijsink, V. G. (2017) Structural diversity of lytic polysaccharide monooxygenases. *Curr. Opin. Struct. Biol.* **44,** 67–76 CrossRef Medline
19. Meier, K. K., Jones, S. M., Kaper, T., Hansson, H., Koetsier, M. J., Karkehabadi, S., Solomon, E. I., Sandgren, M., and Kelemen, B. (2018) Oxygen activation by Cu LPMOs in recalcitrant carbohydrate polysaccharide conversion to monomer sugars. *Chem. Rev.* **118,** 2593–2635 CrossRef Medline
20. Tandrup, T., Frandsen, K. E. H., Johansen, K. S., Berrin, J. G., and Lo Leggio, L. (2018) Recent insights into lytic polysaccharide monooxygenases (LPMOs). *Biochem. Soc. Trans.* **46,** 1431–1447 CrossRef Medline
21. Hu, J., Chandra, R., Arantes, V., Gourlay, K., Susan van Dyk, J., and Saddler, J. N. (2015) The addition of accessory enzymes enhances the hydrolytic performance of cellulase enzymes at high solid loadings. *Bioresour. Technol.* **186,** 149–153 CrossRef Medline
22. Müller, G., Várnai, A., Johansen, K. S., Eijsink, V. G., and Horn, S. J. (2015) Harnessing the potential of LPMO-containing cellulase cocktails poses new demands on processing conditions. *Biotechnol. Biofuels* **8,** 187 CrossRef Medline
23. Chylenski, P., Petrović, D. M., Müller, G., Dahlström, M., Bengtsson, O., Lersch, M., Siika-Aho, M., Horn, S. J., and Eijsink, V. G. H. (2017) Enzymatic degradation of sulfite-pulped softwoods and the role of LPMOs. *Biotechnol. Biofuels* **10,** 177 CrossRef Medline
24. Müller, G., Chylenski, P., Bissaro, B., Eijsink, V. G. H., and Horn, S. J. (2018) The impact of hydrogen peroxide supply on LPMO activity and overall saccharification efficiency of a commercial cellulase cocktail. *Biotechnol. Biofuels* **11,** 209 CrossRef Medline
25. Agger, J. W., Isaksen, T., Várnai, A., Vidal-Melgosa, S., Willats, W. G., Ludwig, R., Horn, S. J., Eijsink, V. G., and Westereng, B. (2014) Discovery of LPMO activity on hemicelluloses shows the importance of oxidative processes in plant cell wall degradation. *Proc. Natl. Acad. Sci. U.S.A.* **111,** 6287–6292 CrossRef Medline
26. Bennati-Granier, C., Garajova, S., Champion, C., Grisel, S., Haon, M., Zhou, S., Fanuel, M., Ropartz, D., Rogniaux, H., Gimbert, I., Record, E., and Berrin, J. G. (2015) Substrate specificity and regioselectivity of fungal AA9 lytic polysaccharide monooxygenases secreted by *Podospora anserina*. *Biotechnol. Biofuels* **8,** 90 CrossRef Medline
27. Vu, V. V., Beeson, W. T., Span, E. A., Farquhar, E. R., and Marletta, M. A. (2014) A family of starch-active polysaccharide monooxygenases. *Proc. Natl. Acad. Sci. U.S.A.* **111,** 13822–13827 CrossRef Medline
28. Lo Leggio, L., Simmons, T. J., Poulsen, J. C., Frandsen, K. E., Hemsworth, G. R., Stringer, M. A., von Freiesleben, P., Tovborg, M., Johansen, K. S., De Maria, L., Harris, P. V., Soong, C. L., Dupree, P., Tryfona, T., Lenfant, N., *et al.* (2015) Structure and boosting activity of a starch-degrading lytic polysaccharide monooxygenase. *Nat. Commun.* **6,** 5961 CrossRef Medline
29. Frommhagen, M., Sforza, S., Westphal, A. H., Visser, J., Hinz, S. W., Koetsier, M. J., van Berkel, W. J., Gruppen, H., and Kabel, M. A. (2015) Discovery of the combined oxidative cleavage of plant xylan and cellulose by a new fungal polysaccharide monooxygenase. *Biotechnol. Biofuels* **8,** 101 CrossRef Medline
30. Couturier, M., Ladevèze, S., Sulzenbacher, G., Ciano, L., Fanuel, M., Moreau, C., Villares, A., Cathala, B., Chaspoul, F., Frandsen, K. E., Labourel, A., Herpoël-Gimbert, I., Grisel, S., Haon, M., Lenfant, N., *et al.* (2018) Lytic xylan oxidases from wood-decay fungi unlock biomass degradation. *Nat. Chem. Biol.* **14,** 306–310 CrossRef Medline
31. Phillips, C. M., Beeson, W. T., Cate, J. H., and Marletta, M. A. (2011) Cellobiose dehydrogenase and a copper-dependent polysaccharide monooxygenase potentiate cellulose degradation by *Neurospora crassa*. *ACS Chem. Biol.* **6,** 1399–1406 CrossRef Medline
32. Westereng, B., Cannella, D., Wittrup Agger, J., Jørgensen, H., Larsen Andersen, M., Eijsink, V. G., and Felby, C. (2015) Enzymatic cellulose oxidation is linked to lignin by long-range electron transfer. *Sci. Rep.* **5,** 18561 CrossRef Medline
33. Beeson, W. T., Phillips, C. M., Cate, J. H., and Marletta, M. A. (2012) Oxidative cleavage of cellulose by fungal copper-dependent polysaccharide monooxygenases. *J. Am. Chem. Soc.* **134,** 890–892 CrossRef Medline
34. Bissaro, B., Røhr, Å. K., Skaugen, M., Forsberg, Z., Horn, S. J., Vaaje-Kolstad, G., and Eijsink, V. (2016) Fenton-type chemistry by a copper enzyme: molecular mechanism of polysaccharide oxidative cleavage. *bioRxiv* CrossRef
35. Bissaro, B., Røhr, Å. K., Müller, G., Chylenski, P., Skaugen, M., Forsberg, Z., Horn, S. J., Vaaje-Kolstad, G., and Eijsink, V. G. H. (2017) Oxidative cleavage of polysaccharides by monocopper enzymes depends on H_2O_2. *Nat. Chem. Biol.* **13,** 1123–1128 CrossRef Medline
36. Kittl, R., Kracher, D., Burgstaller, D., Haltrich, D., and Ludwig, R. (2012) Production of four *Neurospora crassa* lytic polysaccharide monooxygenases in *Pichia pastoris* monitored by a fluorimetric assay. *Biotechnol. Biofuels* **5,** 79 CrossRef Medline
37. Li, X., Beeson, W. T., 4th, Phillips, C. M., Marletta, M. A., and Cate, J. H. (2012) Structural basis for substrate targeting and catalysis by fungal polysaccharide monooxygenases. *Structure* **20,** 1051–1061 CrossRef Medline
38. Vu, V. V., Beeson, W. T., Phillips, C. M., Cate, J. H., and Marletta, M. A. (2014) Determinants of regioselective hydroxylation in the fungal polysaccharide monooxygenases. *J. Am. Chem. Soc.* **136,** 562–565 CrossRef Medline
39. Borisova, A. S., Isaksen, T., Dimarogona, M., Kognole, A. A., Mathiesen, G., Várnai, A., Røhr, Å. K., Payne, C. M., Sørlie, M., Sandgren, M., and Eijsink, V. G. (2015) Structural and functional characterization of a lytic polysaccharide monooxygenase with broad substrate specificity. *J. Biol. Chem.* **290,** 22955–22969 CrossRef Medline
40. Mattinen, M. L., Linder, M., Drakenberg, T., and Annila, A. (1998) Solution structure of the cellulose-binding domain of endoglucanase I from *Trichoderma reesei* and its interaction with cello-oligosaccharides. *Eur. J. Biochem.* **256,** 279–286 CrossRef Medline
41. Boraston, A. B., Bolam, D. N., Gilbert, H. J., and Davies, G. J. (2004) Carbohydrate-binding modules: fine-tuning polysaccharide recognition. *Biochem. J.* **382,** 769–781 CrossRef Medline
42. Isaksen, T., Westereng, B., Aachmann, F. L., Agger, J. W., Kracher, D., Kittl, R., Ludwig, R., Haltrich, D., Eijsink, V. G., and Horn, S. J. (2014) A C4-oxidizing lytic polysaccharide monooxygenase cleaving both cellulose and cello-oligosaccharides. *J. Biol. Chem.* **289,** 2632–2642 CrossRef Medline
43. Kracher, D., Andlar, M., Furtmüller, P. G., and Ludwig, R. (2018) Active-site copper reduction promotes substrate binding of fungal lytic polysaccharide monooxygenase and reduces stability. *J. Biol. Chem.* **293,** 1676–1687 CrossRef Medline
44. Westereng, B., Agger, J. W., Horn, S. J., Vaaje-Kolstad, G., Aachmann, F. L., Stenstrøm, Y. H., and Eijsink, V. G. (2013) Efficient separation of oxidized cello-oligosaccharides generated by cellulose degrading lytic polysaccharide monooxygenases. *J. Chromatogr. A* **1271,** 144–152 CrossRef Medline
45. Wu, M., Beckham, G. T., Larsson, A. M., Ishida, T., Kim, S., Payne, C. M., Himmel, M. E., Crowley, M. F., Horn, S. J., Westereng, B., Igarashi, K., Samejima, M., Ståhlberg, J., Eijsink, V. G., and Sandgren, M. (2013) Crystal structure and computational characterization of the lytic polysaccharide

monooxygenase GH61D from the Basidiomycota fungus *Phanerochaete chrysosporium*. *J. Biol. Chem.* **288,** 12828–12839 CrossRef Medline

46. Courtade, G., Wimmer, R., Røhr, Å. K., Preims, M., Felice, A. K., Dimarogona, M., Vaaje-Kolstad, G., Sørlie, M., Sandgren, M., Ludwig, R., Eijsink, V. G., and Aachmann, F. L. (2016) Interactions of a fungal lytic polysaccharide monooxygenase with beta-glucan substrates and cellobiose dehydrogenase. *Proc. Natl. Acad. Sci. U.S.A.* **113,** 5922–5927 CrossRef Medline
47. Frandsen, K. E., Simmons, T. J., Dupree, P., Poulsen, J. C., Hemsworth, G. R., Ciano, L., Johnston, E. M., Tovborg, M., Johansen, K. S., von Freiesleben, P., Marmuse, L., Fort, S., Cottaz, S., Driguez, H., Henrissat, B., *et al.* (2016) The molecular basis of polysaccharide cleavage by lytic polysaccharide monooxygenases. *Nat. Chem. Biol.* **12,** 298–303 CrossRef Medline
48. Westereng, B., Arntzen, M. Ø., Aachmann, F. L., Várnai, A., Eijsink, V. G., and Agger, J. W. (2016) Simultaneous analysis of C1 and C4 oxidized oligosaccharides, the products of lytic polysaccharide monooxygenases acting on cellulose. *J. Chromatogr. A* **1445,** 46–54 CrossRef Medline
49. Courtade, G., Forsberg, Z., Heggset, E. B., Eijsink, V. G. H., and Aachmann, F. L. (2018) The carbohydrate-binding module and linker of a modular lytic polysaccharide monooxygenase promote localized cellulose oxidation. *J. Biol. Chem.* **293,** 13006–13015 CrossRef Medline
50. Pricelius, S., Ludwig, R., Lant, N., Haltrich, D., and Guebitz, G. M. (2009) Substrate specificity of *Myriococcum thermophilum* cellobiose dehydrogenase on mono-, oligo-, and polysaccharides related to in situ production of H_2O_2. *Appl. Microbiol. Biotechnol.* **85,** 75–83 CrossRef Medline
51. Takeda, K., Matsumura, H., Ishida, T., Samejima, M., Ohno, H., Yoshida, M., Igarashi, K., and Nakamura, N. (2015) Characterization of a novel PQQ-dependent quinohemoprotein pyranose dehydrogenase from *Coprinopsis cinerea* classified into auxiliary activities family 12 in carbohydrate-active enzymes. *PLoS One* **10,** e0115722 CrossRef Medline
52. Hangasky, J. A., Iavarone, A. T., and Marletta, M. A. (2018) Reactivity of O_2 versus H_2O_2 with polysaccharide monooxygenases. *Proc. Natl. Acad. Sci. U.S.A.* **115,** 4915–4920 CrossRef Medline
53. Forsberg, Z., Bissaro, B., Gullesen, J., Dalhus, B., Vaaje-Kolstad, G., and Eijsink, V. G. H. (2018) Structural determinants of bacterial lytic polysaccharide monooxygenase functionality. *J. Biol. Chem.* **293,** 1397–1412 CrossRef Medline
54. Carpita, N. C., and Gibeaut, D. M. (1993) Structural models of primary cell walls in flowering plants: consistency of molecular structure with the physical properties of the walls during growth. *Plant J.* **3,** 1–30 CrossRef Medline
55. Burton, R. A., Gidley, M. J., and Fincher, G. B. (2010) Heterogeneity in the chemistry, structure and function of plant cell walls. *Nat. Chem. Biol.* **6,** 724–732 CrossRef Medline
56. Park, Y. B., and Cosgrove, D. J. (2015) Xyloglucan and its interactions with other components of the growing cell wall. *Plant Cell Physiol.* **56,** 180–194 CrossRef Medline
57. Bissaro, B., Isaksen, I., Vaaje-Kolstad, G., Eijsink, V. G. H., and Røhr, Å. K. (2018) How a lytic polysaccharide monooxygenase binds crystalline chitin. *Biochemistry* **57,** 1893–1906 CrossRef Medline
58. Frommhagen, M., Koetsier, M. J., Westphal, A. H., Visser, J., Hinz, S. W., Vincken, J. P., van Berkel, W. J., Kabel, M. A., and Gruppen, H. (2016) Lytic polysaccharide monooxygenases from *Myceliophthora thermophila* C1 differ in substrate preference and reducing agent specificity. *Biotechnol. Biofuels* **9,** 186 CrossRef Medline
59. Frommhagen, M., Westphal, A. H., van Berkel, W. J. H., and Kabel, M. A. (2018) Distinct substrate specificities and electron-donating systems of fungal lytic polysaccharide monooxygenases. *Front. Microbiol.* **9,** 1080 CrossRef Medline
60. Várnai, A., Umezawa, K., Yoshida, M., and Eijsink, V. G. H. (2018) The pyrroloquinoline-quinone dependent pyranose dehydrogenase from *Coprinopsis cinerea* (*Cc*PDH) drives lytic polysaccharide monooxygenase (LPMO) action. *Appl. Environ. Microbiol.* **84,** e00156-18 CrossRef Medline
61. Zhang, J., Presley, G. N., Hammel, K. E., Ryu, J. S., Menke, J. R., Figueroa, M., Hu, D., Orr, G., and Schilling, J. S. (2016) Localizing gene regulation reveals a staggered wood decay mechanism for the brown rot fungus *Postia placenta*. *Proc. Natl. Acad. Sci. U.S.A.* **113,** 10968–10973 CrossRef Medline
62. Wood, T. M. (1988) Preparation of crystalline, amorphous, and dyed cellulase substrates, in *Methods in Enzymology* (Wood, W. A., and Kellogg, S. T., eds) pp. 19–25, Academic Press, San Diego
63. Zámocký, M., Schümann, C., Sygmund, C., O'Callaghan, J., Dobson, A. D., Ludwig, R., Haltrich, D., and Peterbauer, C. K. (2008) Cloning, sequence analysis and heterologous expression in *Pichia pastoris* of a gene encoding a thermostable cellobiose dehydrogenase from *Myriococcum thermophilum*. *Protein Expr. Purif.* **59,** 258–265 CrossRef Medline
64. Matsumura, H., Umezawa, K., Takeda, K., Sugimoto, N., Ishida, T., Samejima, M., Ohno, H., Yoshida, M., Igarashi, K., and Nakamura, N. (2014) Discovery of a eukaryotic pyrroloquinoline quinone-dependent oxidoreductase belonging to a new auxiliary activity family in the database of carbohydrate-active enzymes. *PLoS One* **9,** e104851 CrossRef Medline
65. Gasteiger, E., Hoogland, C., Gattiker, A., Duvaud, S. e., Wilkins, M. R., Appel, R. D., and Bairoch, A. (2005) Protein identification and analysis tools on the ExPASy server, in *The Proteomics Protocols Handbook* (Walker, J. M., ed) pp. 571–607, Humana Press, Totowa, NJ
66. Várnai, A., Tang, C., Bengtsson, O., Atterton, A., Mathiesen, G., and Eijsink, V. G. (2014) Expression of endoglucanases in *Pichia pastoris* under control of the GAP promoter. *Microb. Cell Fact.* **13,** 57 CrossRef Medline
67. Sygmund, C., Kracher, D., Scheiblbrandner, S., Zahma, K., Felice, A. K., Harreither, W., Kittl, R., and Ludwig, R. (2012) Characterization of the two *Neurospora crassa* cellobiose dehydrogenases and their connection to oxidative cellulose degradation. *Appl. Environ. Microbiol.* **78,** 6161–6171 CrossRef Medline
68. Loose, J. S., Forsberg, Z., Fraaije, M. W., Eijsink, V. G., and Vaaje-Kolstad, G. (2014) A rapid quantitative activity assay shows that the *Vibrio cholerae* colonization factor GbpA is an active lytic polysaccharide monooxygenase. *FEBS Lett.* **588,** 3435–3440 CrossRef Medline
69. Kabsch, W. (2010) XDS. *Acta Crystallogr. D Biol. Crystallogr.* **66,** 125–132 CrossRef Medline
70. McCoy, A. J., Grosse-Kunstleve, R. W., Adams, P. D., Winn, M. D., Storoni, L. C., and Read, R. J. (2007) Phaser crystallographic software. *J. Appl. Crystallogr.* **40,** 658–674 CrossRef Medline
71. Stein, N. (2008) CHAINSAW: a program for mutating pdb files used as templates in molecular replacement. *J. Appl. Crystallogr.* **41,** 641–643 CrossRef
72. Emsley, P., Lohkamp, B., Scott, W. G., and Cowtan, K. (2010) Features and development of Coot. *Acta Crystallogr. D Biol. Crystallogr.* **66,** 486–501 CrossRef Medline
73. Murshudov, G. N., Vagin, A. A., and Dodson, E. J. (1997) Refinement of macromolecular structures by the maximum-likelihood method. *Acta Crystallogr. D Biol. Crystallogr.* **53,** 240–255 CrossRef Medline
74. Chen, V. B., Arendall, W. B., 3rd, Headd, J. J., Keedy, D. A., Immormino, R. M., Kapral, G. J., Murray, L. W., Richardson, J. S., and Richardson, D. C. (2010) MolProbity: all-atom structure validation for macromolecular crystallography. *Acta Crystallogr. D Biol. Crystallogr.* **66,** 12–21 CrossRef Medline
75. Pettersen, E. F., Goddard, T. D., Huang, C. C., Couch, G. S., Greenblatt, D. M., Meng, E. C., and Ferrin, T. E. (2004) UCSF Chimera—a visualization system for exploratory research and analysis. *J. Comput. Chem.* **25,** 1605–1612 CrossRef Medline
76. Forsberg, Z., Nelson, C. E., Dalhus, B., Mekasha, S., Loose, J. S., Crouch, L. I., Røhr, Å. K., Gardner, J. G., Eijsink, V. G., and Vaaje-Kolstad, G. (2016) Structural and functional analysis of a lytic polysaccharide monooxygenase important for efficient utilization of chitin in *Cellvibrio japonicus*. *J. Biol. Chem.* **291,** 7300–7312 CrossRef Medline
77. Strohalm, M., Kavan, D., Novák, P., Volný, M., and Havlícek, V. (2010) mMass 3: a cross-platform software environment for precise analysis of mass spectrometric data. *Anal. Chem.* **82,** 4648–4651 CrossRef Medline
78. Petrović, D. M., Bissaro, B., Chylenski, P., Skaugen, M., Sørlie, M., Jensen, M. S., Aachmann, F. L., Courtade, G., Várnai, A., and Eijsink, V. G. H. (2018) Methylation of the N-terminal histidine protects a lytic polysaccharide monooxygenase from auto-oxidative inactivation. *Protein Sci.* **27,** 1636–1650 CrossRef Medline
79. Nekiunaite, L., Petrović, D. M., Westereng, B., Vaaje-Kolstad, G., Hachem, M. A., Várnai, A., and Eijsink, V. G. (2016) *Fg*LPMO9A from *Fusarium graminearum* cleaves xyloglucan independently of the backbone substitution pattern. *FEBS Lett.* **590,** 3346–3356 CrossRef Medline